

Piotr TYCZYŃSKI^a, Zbigniew SIEMIĄTKOWSKI^{b,*}, Mirosław RUCKI^b

^a Mapal Narzędzia Precyzyjne Sp. z o.o., Poznań, Poland

^b Faculty of Mechanical Engineering, Kazimierz Pułaski University of Technology and Humanities in Radom, Poland

* Corresponding author: z.siemiatkowski@uthrad.pl

DRILL BASE BODY FABRICATED WITH ADDITIVE MANUFACTURING TECHNOLOGY: STRUCTURE, STRENGTH AND RELIABILITY

© 2019 Piotr Tyczyński, Zbigniew Siemiątkowski, Mirosław Ruck

This is an open access article licensed under the Creative Commons Attribution International License (CC BY)

 <https://creativecommons.org/licenses/by/4.0/>

Key words: additive manufacturing, selective laser melting, porosity, drilling, drill body design, coolant ducts.

Abstract: The paper presents an investigation of results on an additive manufactured drill base body. Due to the technological and strength limitations, conventional drills with inner coolant ducts may not be smaller than 13 mm diameter. The novel idea was to keep the strength of small diameter drills making spiral coolant ducts. Drills were fabricated using a 3D laser printer to obtain the designed geometry in a way not affecting its stiffness and strength. The tensile strength of samples was between $R_m = 1287$ and 1603 MPa, and microhardness of drills was between 606 and 627 HV5. The sintered material revealed a very small porosity rate (below 1%) and very few discontinuities. Thus, it was demonstrated that the 3D laser printing enabled the production of advantageous drill base bodies.

Korpus wiertła wykonany za pomocą technologii addytywnej: struktura, wytrzymałość i trwałość

Słowa kluczowe: technologie addytywne, technologia selektywnego topienia laserowego, porowatość, wiercenie, konstrukcja korpusu wiertła, kanały chłodzące.

Streszczenie: W artykule przedstawiono wyniki badań korpusu wiertła wykonanego za pomocą technologii addytywnej. Ze względu na ograniczenia technologiczne i wytrzymałościowe tradycyjne wiertła z wewnętrznymi kanałami nie mogą mieć średnic mniejszych niż 13 mm. Zaprojektowano nowatorskie wiertła o mniejszych średnicach ze spiralnymi kanałami wewnętrznymi, które w mniejszym stopniu obniżają wytrzymałość korpusu. Wykonano je za pomocą laserowej drukarki 3D, gdyż uzyskanie takiego kształtu technologią tradycyjną jest bardzo utrudnione. Wytrzymałość próbek uzyskano w granicach od $R_m = 1287$ do 1603 MPa, a mikrotwierdź pomiędzy 606 a 627 HV5. Uzyskany materiał wykazywał bardzo małą porowatość poniżej 1% i bardzo niewiele nieciągłości struktury. W ten sposób wykazano, że laserowy druk 3D daje możliwość wykonania korpusów wiertel o wysokiej wytrzymałości.

Introduction

Additive Manufacturing (AM) technologies are opening new opportunities in terms of the production paradigm and manufacturing possibilities [1]. Commonly known as “three-dimensional (3D) printing,” it is a recently invented computer dependent technology that has proven its success as an option for production of parts in a wide application range [2]. These are often highly complexity items, which could be very difficult or even impossible to be manufactured by other processes [3]. The absence of waste material, like chips resulting from machining, is also a great AM advantage in terms

of saving energy, material, tooling, and man power. It is considered more environmental friendly even though, for most AM processes, 3D printers use more energy than that of comparable conventional processes at process or machine levels [4]. In particular, selective laser melting demonstrated its enormous potential on generating functional structures and complex geometries through layer-by-layer fabrication [5].

“Rapid tooling” describes the additive manufacturing of tools, tool inserts, gauges, and moulds. The additive manufacturing of tool inserts is older than those of final products and was introduced in the early 1990s [6]. In the last decade, some companies started to deliver machine tools with replaceable inserts fixed in the holders

produced using the additive manufacturing processes [7]. Within the space of the laser printer, tool geometries can be created unhindered by machine clamps, tools, and production means [8].

The present study is dedicated to a drill base body made out of Maraging Steel 1.2709 fabricated with selective laser melting (SLM) technology [9]. This method can be described as a rapid manufacturing process and consists of the consolidation of various materials with a laser beam [10]. Several methods were proposed to monitor and in-process control the quality of the produced details, e.g., image data analysis that enabled the detection of structural defects [11].

Recent research provided interesting results on the general microstructure and mechanical properties of maraging steel after the SLM process and post heat treatment [12]. Other teams examined its tensile, fracture, and fatigue strength [13], microstructural evolution, nano-precipitation behaviour, and mechanical properties [14] as well as the influence of scan length on the properties of the thin-walled components [15]. In the present study, the strength and microstructure of the drill base body was examined in order to demonstrate that SLM technology is advantageous in the fabrication of these specific tools.

1. AM design of drill body

In the case of higher requirements for productivity and quality, through-tool metalworking fluids (MWF) systems are applied [16]. Tool holders with integrated extension arms are used, which are widely available from major drilling tool suppliers. When a through-MWF tool is connected to a properly equipped tool holder, the fluid flows through the tool's internal channels and out of the tool's nozzles. Drills with coolant ducts are capable of pressing the coolant directly into the cutting position [17]. The required flow rate is assured by high MWF pressure up to 250 bar and by the optimized cross-section of the internal channel [18]. However, larger cross-sections of coolant ducts lead to a decrease in the wall thickness, which makes the tool fragile. Additionally, the base body is weakened by the openings for the screws or other elements holding the inserts. Until recently, these drills were only offered in diameters of 13 mm or larger, because central coolant supply channels with Y-shaped outlets substantially reduced their strength [19].

Several models of the cooling lubricant flow were proposed, which is very important for understanding and providing sufficient cooling, and to help optimizing the arrangements of the internal coolant channels [20]. Normally, the friction in the helical channel is greater than that for straight duct [16]. Nevertheless, the flow inside helical drill coolant channel has been demonstrated to have a small dependence on angular velocity [21]. Moreover, the helical ducts placed along the flutes in the drill bodies fabricated with 3D printing technology did

not weaken the drill core. Figure 1 presents a view of the SLM produced drill body and its tomography.

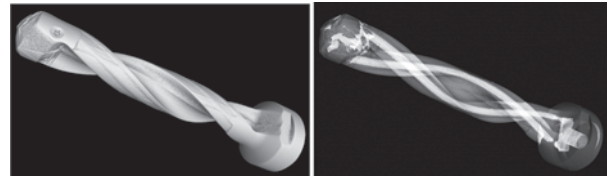


Fig. 1. Helical coolant ducts inside the drill base body

Layer-by-layer AM technology enables one to keep the coolant ducts diameters large enough for proper coolant flow, despite the small diameters of the drill itself. Moreover, the intersection of the coolant channel can be designed in any shape, e.g., the triangle shown in Fig. 2, which is absolutely unachievable in conventional technologies. In this way, it is possible to produce the insert drills with diameters as small as 8 mm, while keeping them strong.

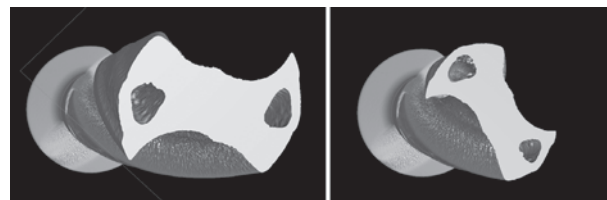


Fig. 2. Two intersections of the drill base body demonstrate a semi-triangle shape of the coolant ducts

The strength of the produced samples was calculated using the Finite Element Method (FEM). The analysis proved that the inner stresses in the drill base body fabricated in AM technology are ca. 50% smaller than that in the conventionally made ones. Figure 3 presents an example where inner stresses of the 3D-printed drill base body with triangle channels reach 820 MPa, while the ones for conventional steel drill base body of similar dimensions shown in Fig. 4 are as large as 1688.3 MPa [9].

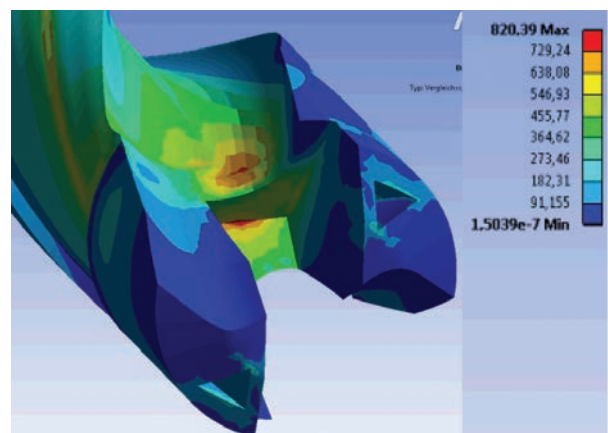


Fig. 3. Example of FEM analysis of the inner stresses in the 3D-printed drill base body [9]

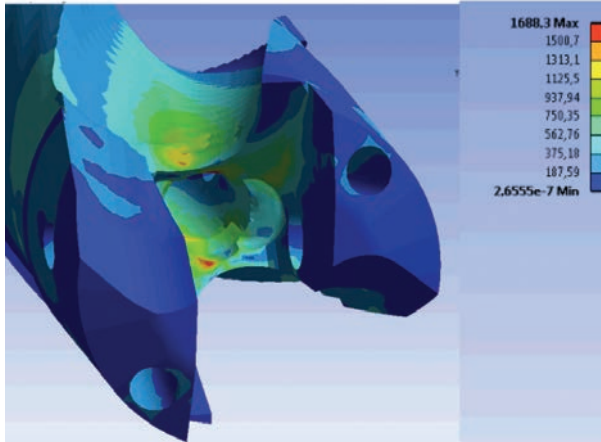


Fig. 4. Example of FEM analysis of the inner stresses in the conventionally fabricated drill base body [9]

2. Experimental conditions

The structure of the drill body was examined in order to determine its homogeneity and porosity, as well as microhardness. These features are very important for the drill's performance.

An Olympus BX51M microscope was used for metallographic analysis. The device enabled us to obtain the images in different lights, namely, white light, direct or reflected light, and polarized light, as well as in the interference contrast. The steady, stable, and shadeless exposition of the sample surface was ensured by a Koehler lighting system with smooth

regulation in the entire range. The surfaces exposed to the measurement were etched with 1% Nital. A camera adapter enabled capturing images and helped to perform acquisition, archiving, and morphometric measurements. Olympus Stream Essentials software was used in order to assess the porosity, i.e. percentage of the pores in the material structure. In Figure 5, a cross-section of the analysed drill body is shown with Points 1, 2, and 3 indicating where the porosity was measured. Figures 6a, b, and c present the images of its structure in the respective Points 1, 2, and 3. Red stains represent pores.

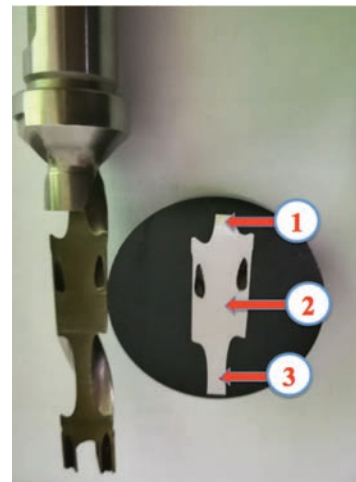


Fig. 5. The examined drill body prepared for porosity and microhardness measurements

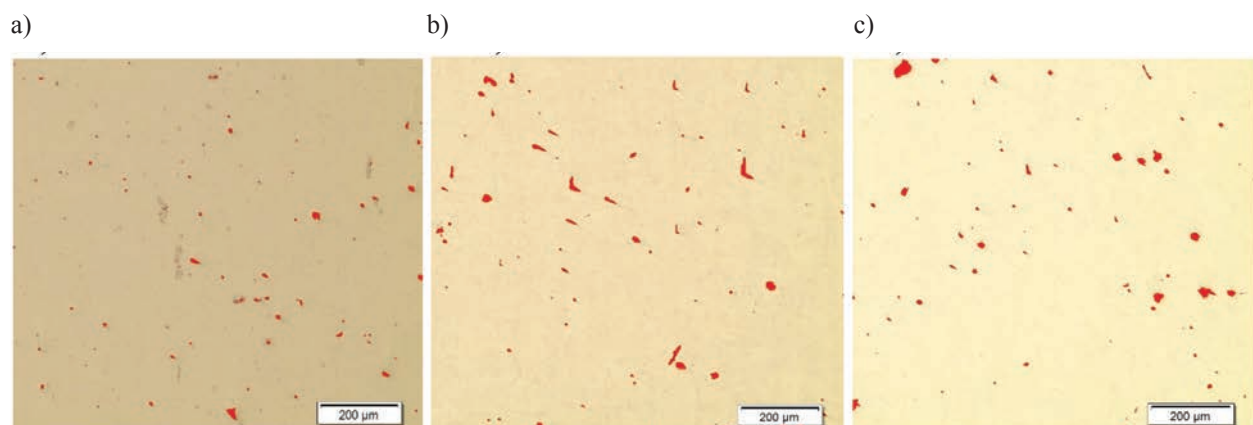


Fig. 6. Images of the drill body structure in the respective points

The hardness of the drill body fabricated with the SLM method was measured with a Qness Q250MS type device. The device is designed for the measurement of Brinell hardness according to the standard DIN EN ISO 6506, Vickers hardness (DIN EN ISO 6506), Rockwell hardness (DIN EN ISO 6508), and Koop microhardness (DIN EN ISO 4545). In the current research, the

methods HV5 and HV0.5 were applied. The former measurement was made in the points specified in Fig. 5, while the latter was repeated 50 times through the entire cross-section of the drill body. The distances between the points of HV0.5 microhardness were ca. 0.2 mm, as seen in Fig. 7.

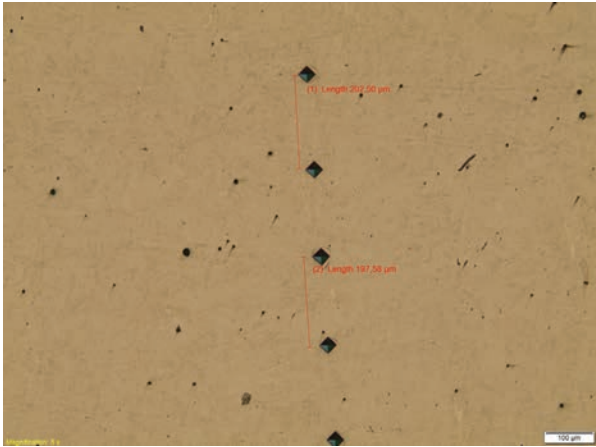


Fig. 7. HV0.5 microhardness measurement

Standard tensile testing was performed with an Instron 3382 device, according to the procedure described in PN-EN ISO 6892-1:2016-09. The 3382 Floor Model Universal Testing System has capacity up to 100 kN and maximum speed 500 mm/min. The force range is 100:1, i.e. using the load cell to 1.0% of its capacity causes no loss of accuracy. The Instron 3382 ensures the load accuracy at the level of 0.5% of the indicated load.

Moreover, fatigue tests were carried out in the laboratory of Rzeszow University of Technology, in accordance with the standard ASTM E466-15. The INSTRON 8801 device was used for the tests at room temperature. The samples underwent the sinusoidal alternating load with frequency of $f = 3$ Hz in conditions of one-sided tensile testing, where the tensions did not change their direction. The cycle asymmetry factor was $\sigma_{\min}/\sigma_{\max} = 0.05$. The maximal stress $\sigma_{\max} = 250$ MPa caused the destruction of the sample after 111,361 cycles, while at $\sigma_{\max} = 210$ MPa, the sample did not break even after 300,000 of cycles. Thus, it can be assumed that for the number of cycles $N_g > 300,000$, the expected fatigue strength of steel 1.2709 details made with SLM technology, in the one-sided tensile conditions, is between 210–250 MPa.

3. Results and discussion

3.1. Microstructure

The porosity of material at Points 1, 2, and 3 were calculated from the microstructure images shown in Figs. 6a, b and c, respectively. The pores percentage calculated by a Stream Essentials program was 0.35% for the Point 1, 0.87% for the Point 2 and 0.74% for the Point 3. As it is seen in Fig. 5, Point 1 with smaller percentage of pores is situated close to the drill holder. The rest of drill body reveals twice as many pores as the area represented by Point 1.

Apart from percentage, the influence of the pores on the drill performance is determined by their shapes and dimensions. Figure 8 presents the examples of pore analysis, where two pores of dimensions $37 \times 38 \mu\text{m}$ and $29 \times 39 \mu\text{m}$ are seen on the typical structure of the material with distinguishable curved melt pool lines. The latter correspond to the locally melted and rapidly solidified regions exposed to scanning laser irradiation [22]. In some cases, the pores had a more irregular shape as seen in Fig. 9, where the pores are slot-like along the melt pool lines. Here, the length of an area with pores forming a discontinuity chain is ca. 220 μm .

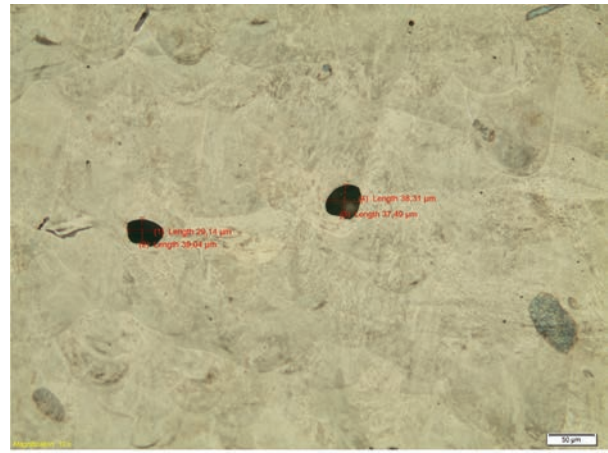


Fig. 8. Photomicrograph of the drill body intersection with semi-round pores

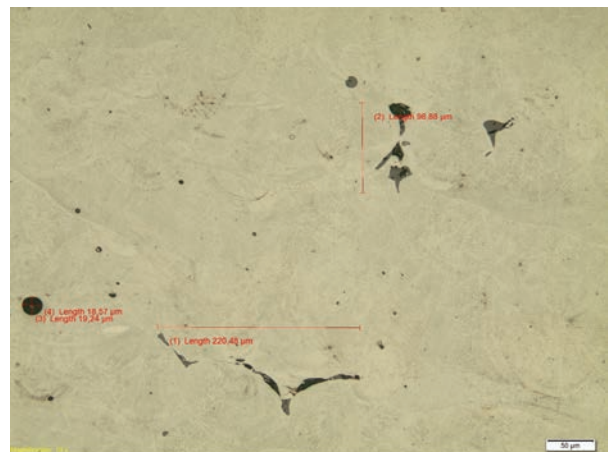


Fig. 9. Photomicrograph of the drill body intersection with pores formed along the melt pool lines

The globular pores were found throughout the entire surface of the analysed intersection. It was noted that they appeared more densely around the holes and close to the edges. The maximal dimension of a pore of this kind was 40 μm . Irregular shaped pores formed along the melt pool lines appeared rarely, and their length was typically below 220 μm .

In addition, the microstructure of edges should be mentioned. Especially in the case of the coolant ducts, the surface microstructure can heavily influence the thermal conditions of drilling process. Figure 10 illustrates how the surface of inner channels is formed.

Asperities made of melted material like dripstones stretch from the surface of coolant ducts. Their height, as seen in the photomicrographs, is ca. 140–180 μm , but some over 0.4 mm can be found. These are undesirable, since they may increase the coolant flow resistance.

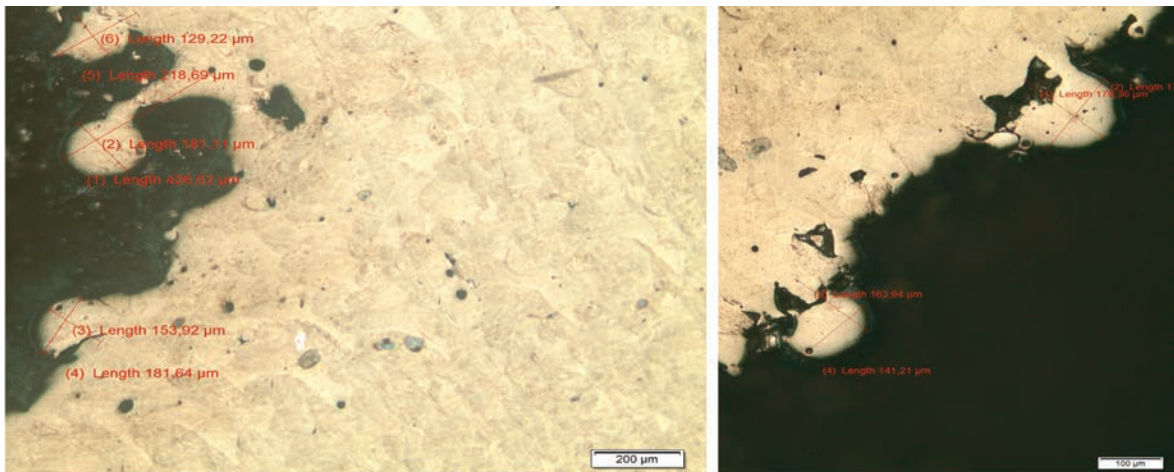


Fig. 10. Photomicrographs of the drill body coolant channels edges

3.2. Microhardness

Results of HV5 measurements are presented in Table 1.

Table 1. Microhardness at the points specified in Fig. 5

Point No.	Value	Method	Lens
1	627	HV5	20×
2	606	HV5	20×
3	619	HV5	20×

The results of microhardness measurement did not vary substantially in the measurement points and did not reveal any trend toward the drill holder or in the opposite direction. Its mean value was 617.3, and its range was $R = 21$, which is ca. 3% of the measured value.

Measurements in 50 subsequent points confirmed the high uniformity of hardness in the entire drill body. The results are presented graphically in Fig. 11.

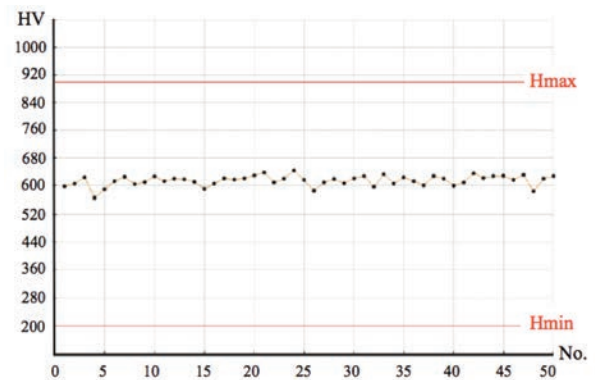


Fig. 11. Microhardness HV0.5 measured at the points specified in Fig. 7

Statistically, the measurement results revealed a very small standard deviation of $s = 15.1$ and a range of $R = 79$. The mean value was 614.3 HV0.5. The steady distribution of the hardness implies the uniformity of the drill body structure and suggests its strength [23, 24].

3.3. Strength of the material

Strain-stress curves for 5 samples of nominal diameter $d_0 = 6.0$ mm and gage length $l_0 = 25$ mm are shown in Fig. 10.

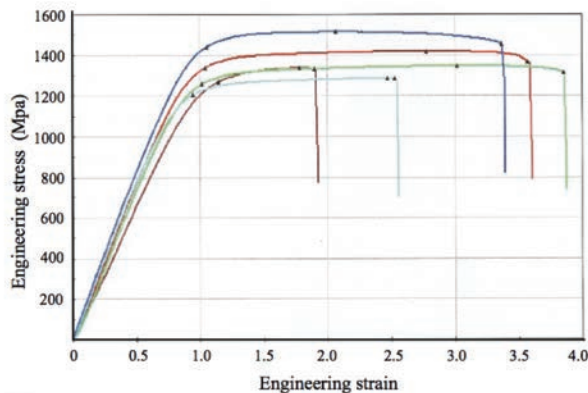


Fig. 12. Example of the strain-stress curves for maraging steel

The samples presented in Fig. 12 revealed a tensile strength between $R_m = 1290$ and 1520 MPa. However, a larger number of tested samples provided a much wider span of R_m values from 1287 up to 1603 MPa with a range of $R = 316$ MPa and a standard deviation of 97 MPa. The variations can be caused by the SLM production technology itself, because the layer-by-layer melting process generated a differentiated microstructure that remained layered despite the application of additional procedures. In the tested series, no correlation was noted between the microstructures and the strength, which may become the objective of further research.

Conclusions

The presented work demonstrated how additive technology could be applied in the production of a drill base body. The novel idea was to achieve spiral coolant ducts along the flutes without weakening the drill core. The research was aimed at assessing the strength and structure of the maraging steel drill bodies produced out of powder with SLM additive technology. The following conclusions can be made:

- 1) Standard strength and fatigue tests proved the good characteristics of the material, even though the tensile strength R_m varied to a high degree for different samples.
- 2) The microstructure of the drill body revealed uniform porosity with a little higher pore percentage at the edges, and smaller percentage of pores close to the drill holder. Occasionally, larger pores in form of slots along the melt pool lines appeared.
- 3) Microhardness HV0.5 measured on the entire length of the drill body proved the highly uniform properties of the detail.

Some problem with the application of the SLM technology for drill base body with inner coolant ducts was posed by the structure of the surface of the channels. High asperities may significantly increase the flow

resistance, which may worsen the cooling conditions of the drilling process. However, the merit from spiral coolant ducts is much more important, because they enable one to fabricate drills of much smaller diameters than that with straight ducts made using conventional technologies. The SLM production of drill base bodies, however, seemed to be limited to ca. 8 mm diameter. Thinner drills did not ensure the required strength.

From the practical perspective, the study demonstrated good properties of the 3D printed maraging steel drill base bodies. They may successfully replace the traditional drills with inner coolant ducts produced with other technologies.

No clear correlation between the microstructure and the strength was noted, so the issue should be addressed in future research.

Acknowledgement

The research was made in the frames of project “New generation of the hydraulic cylinder FBW made with application of Additive Manufacturing and machining technology at low temperatures (cryogenics),” Activity 1.2 of Sector Programs B+R, POIR 2014-2020, project No. POIR.01.02.00-00-0010/15.

References

1. Attaran M.: The rise of 3-D printing: The advantages of additive manufacturing over traditional manufacturing. *Business Horizons*, 2017, 60(5), pp. 677–688, DOI: 10.1016/j.bushor.2017.05.011.
2. DebRoy T., Wei H.L., Zuback J.S., Mukherjee T., Elmer J.W., Milewski J.O., Beese A.M., Wilson-Heid A., De A., Zhang W.: Additive manufacturing of metallic components – Process, structure and properties. *Progress in Materials Science*, 2018, 92, pp. 112–224, DOI: 10.1016/j.pmatsci.2017.10.001.
3. Umaras E., Tsuzuki M.S.G.: Additive Manufacturing – Considerations on Geometric Accuracy and Factors of Influence. *IFAC PapersOnLine*, 2017, 50(1), pp. 14940–14945, DOI: 10.1016/j.ifacol.2017.08.2545.
4. Rejeski D., Zhao F., Huang Y.: Research needs and recommendations on environmental implications of additive manufacturing. *Additive Manufacturing*, 2018, 19, pp. 21–28, DOI: 10.1016/j.addma.2017.10.019.
5. Zhang J., Tai W.G., Wang H., Kumar A.S., Lu W.F., Fuh J.Y.H.: Magnetic abrasive polishing of additively manufactured 316L stainless steel parts. *Euspen's 18th International Conference & Exhibition 4-8 June 2018, Venice (Italy)*. Proceedings, pp. 401–402.

6. Gebhardt A., Hötter J.S.: *Additive Manufacturing*. Munich: Hanser Publishers, 2016.
7. Sandvik Coromant: *Main website*. Online.. 2017. Accessed 30 December 2017. Available from: www.sandvik.coromant.com
8. Mapal: *Main website*. Online. 2017. Accessed 30 December 2017.. Available from: www.mapal.com
9. Tyczyński P., Siemiątkowski Z., Rucki M.: Analysis of the drill base body fabricated with Additive Manufacturing technology. *Euspen's 18th International Conference & Exhibition 4–8 June 2018, Venice (Italy)*. Proceedings, pp. 287–288.
10. Xue L.: *Laser Consolidation – A Rapid Manufacturing Process for Making Net-Shape Functional Components*. In: Lawrence J. (ed.): *Advances in Laser Materials Processing: Technology, Research and Applications*, 2nd edition, London: Woodhead Publishing, 2018, pp. 461–505.
11. Grasso M., Caltanissetta F., Petrò S., Colosimo B.M.: In-situ Monitoring of Geometric Accuracy in Laser Powder Bed Fusion processes. *Euspen's 18th International Conference & Exhibition 4–8 June 2018, Venice (Italy)*. Proceedings, pp. 293–294.
12. Mutua J., Nakata Sh., Onda T., Chen Zh.Ch.: Optimization of selective laser melting parameters and influence of post heat treatment on microstructure and mechanical properties of maraging steel. *Materials & Design*, 2018, 139, pp. 486–497, DOI: 10.1016/j.matdes.2017.11.042.
13. Suryawanshi J., Prashanth K.G., Ramamurty U.: Tensile, fracture, and fatigue crack growth properties of a 3D printed maraging steel through selective laser melting. *Journal of Alloys and Compounds*, 2017, 725, pp. 355–364, DOI: 10.1016/j.jallcom.2017.07.177.
14. Tan Ch., Zhou K., Ma W., Zhang P., Kuang T.: Microstructural evolution, nanoprecipitation behavior and mechanical properties of selective laser melted high-performance grade 300 maraging steel. *Materials & Design*, 2017, 134, pp. 23–34, DOI: 10.1016/j.matdes.2017.08.026.
15. Li Zh., Xu R., Zhang Zh., Kucukkoc I.: The influence of scan length on fabricating thin-walled components in selective laser melting. *International Journal of Machine Tools and Manufacture*, 2018, 126, pp. 1–12, DOI: 10.1016/j.ijmachtools.2017.11.012.
16. Astakhov V.P.: *Drills: Science and Technology of Advanced Operations*. Boca Raton: CRC Press, 2014.
17. Tschätsch H.: *Applied Machining Technology*. Heidelberg – London: Springer, 2009.
18. Heisel U., Stortchak M., Eisseler R.: *Optimization of Deep Hole Drilling Processes with Smallest Drilling Diameters*. In: Inasaki I. (ed.): *Initiatives of Precision Engineering at the Beginning of a Millennium*. New York: Kluwer Academic Publishers, 2002, pp. 157–163.
19. Hendrixson S.: *Additive Manufacturing Makes Subtractive Cutting Tools*. Online.. 2015. Accessed 9 July 2018.. Available from: <https://www.additivemanufacturing.media/articles/additive-manufacturing-makes-subtractive-cutting-tools>
20. Schnabel D., Özkay E., Biermann D., Eberhard P.: Modeling the motion of the cooling lubricant in drilling processes using the finite volume and the smoothed particle hydrodynamics methods. *Computer Methods in Applied Mechanics and Engineering*, 2018, 329, pp. 369–395, DOI: 10.1016/j.cma.2017.09.015.
21. Johns A.S., Hewson R.W., Merson E., Summers J.L., Thompson H.M.: *Internal twist drill coolant channel modelling using computational fluid dynamics*. In: Oñate E., Oliver J., Huerta A. (eds.): *Proceedings of 6th European Conference on Computational Fluid Dynamics (ECFD)*, 2014, II, pp. 1114–1122.
22. Takata N., Nishida R., Suzuki A., Kobashi M., Kato M.: Crystallographic Features of Microstructure in Maraging Steel Fabricated by Selective Laser Melting. *Metals*, 2018, 8, pp. 440–450, DOI: 10.3390/met8060440.
23. Umemoto M., Liu Z.G., Tsuchiya K., Sugimoto S., Bepari M.M.A.: Relationship between hardness and tensile properties in various single structured steels. *Materials Science and Technology*, 2001, 17(5), pp. 505–511, DOI: 10.1179/026708301101510339.
24. Zhang P., Li S.X., Zhang Z.F.: General relationship between strength and hardness. *Materials Science and Engineering: A*, 2011, 529(25), pp. 62–73, DOI: 10.1016/j.msea.2011.08.061.

This article appeared in its printed version in Journal of Machine Construction and Maintenance. The electronic version is published in DEStech Publications, Inc., Lancaster, PA, 2019, Proceedings of FUTURE ENGINEERING CONFERENCE.